

PREPARED FOR SUBMISSION TO JINST

N<sup>TH</sup> WORKSHOP ON X

WHEN

WHERE

## Developments and improvements of radiopure ZnWO<sub>4</sub> anisotropic scintillators

---

**P. Belli<sup>a,b</sup> R. Bernabei<sup>a,b</sup> F. Cappella<sup>c,d</sup> V. Caracciolo<sup>a,b,e</sup> R. Cerulli<sup>a,b</sup> N. Cherubini<sup>f</sup>  
F. A. Danevich<sup>g</sup> A. Incicchitti<sup>c,d</sup> D. V. Kasperovych<sup>g</sup> V. Merlo<sup>a,b</sup> E. Piccinelli<sup>f</sup>  
O. G. Polischuk<sup>g</sup> V. I. Tretyak<sup>g</sup>**

<sup>a</sup>INFN sezione Roma “Tor Vergata”, I-00133 Rome, Italy

<sup>b</sup>Dipartimento di Fisica, Università di Roma “Tor Vergata”, I-00133, Rome, Italy

<sup>c</sup>INFN sezione Roma, I-00185 Rome, Italy

<sup>d</sup>Dipartimento di Fisica, Università di Roma “La Sapienza”, I-00185 Rome, Italy

<sup>e</sup>INFN, Laboratori Nazionali del Gran Sasso, I-67100 Assergi (AQ), Italy

<sup>f</sup>Enea, Italian National Agency for New Technologies, Energy and Sustainable Economic Development, C.R.: Casaccia, Roma 00123, Italy

<sup>g</sup>Institute for Nuclear Research, 03028 Kyiv, Ukraine

E-mail: [riccardo.cerulli@roma2.infn.it](mailto:riccardo.cerulli@roma2.infn.it)

**ABSTRACT:** The ZnWO<sub>4</sub> is an anisotropic crystal scintillator; for its peculiar characteristics, it is a very promising detector to exploit the so-called directionality approach in the investigation of those Dark Matter (DM) candidates inducing nuclear recoils. Recently, in the framework of the ADAMO project, an R&D to develop high quality and ultra-radiopure ZnWO<sub>4</sub> crystal scintillators has been carried out. In the present paper the measurements to study the anisotropic response of a ZnWO<sub>4</sub> to  $\alpha$  particles and to nuclear recoils induced by neutron scattering are reported. Monochromatic neutrons have been produced by a neutron generator at ENEA-CASACCIA. The quenching factor values for nuclear recoils along different crystallographic axes have been determined for three different nuclear recoils energies. These results open the possibility to realize a pioneer experiment to investigate the above mentioned DM candidates by means of the directionality.

**KEYWORDS:** Dark Matter detectors, Scintillators

---

## Contents

<b>1</b>	<b>Introduction</b>	<b>1</b>
<b>2</b>	<b>ZnWO<sub>4</sub> anisotropic scintillator</b>	<b>1</b>
<b>3</b>	<b>Measurements with <math>\alpha</math> particles</b>	<b>2</b>
<b>4</b>	<b>Measurements with neutrons</b>	<b>4</b>
<b>5</b>	<b>Conclusions</b>	<b>8</b>

---

## 1 Introduction

The presence of Dark Matter (DM) candidates inducing nuclear recoils can be investigated by exploiting the so called directionality approach based on the correlation between the direction of nuclear recoils in the target detector and the impinging direction of the DM wind in the Galactic halo. This approach can be complementary to the model independent annual modulation signature that has been successfully exploited by the DAMA/NaI, DAMA/LIBRA-phase1 and DAMA/LIBRA-phase2 experiments giving a positive model independent result with high confidence level [1–6].

The idea to use anisotropic crystal scintillators to pursue the directionality approach was proposed in Ref. [7, 8]. The light output of the anisotropic scintillators for heavy particles ( $p$ ,  $\alpha$ , nuclear recoils) depends on the direction of the particles with respect to the crystal axes. This offers a possibility to point out the presence of heavy ionizing particles with a preferred direction (such as recoil nuclei induced by DM candidates interaction) with respect to the electromagnetic background by comparing the low energy distributions measured using different orientations of the crystal axes during the day [7–9]. The ZnWO<sub>4</sub> is a very promising crystal for this purpose offering suitable features [9–15]. This motivated the proposal of ADAMO (Anisotropic detectors for DArk Matter Observation), a project to perform an R&D to develop low background, high quality ZnWO<sub>4</sub> crystals for a pioneering experiment to investigate the directionality [9, 15–18]. In this paper the recent results of the R&Ds will be briefly presented with particular regard to the recent measurements performed with a neutron generator at ENEA-CASACCIA [19].

## 2 ZnWO<sub>4</sub> anisotropic scintillator

In the last years several ZnWO<sub>4</sub> detectors have been developed in the framework of the collaboration between the DAMA group of INFN and the INR-Kyiv group [11, 12, 20, 21]. Formerly, some crystals were produced by the Institute for Scintillation Materials (ISMA, Kharkiv, Ukraine) and, later on, a collaboration with the Nikolaev Institute of Inorganic Chemistry (Novosibirsk, Russia) has started. In this last Collaboration a R&D to produce ultra-radiopure ZnWO<sub>4</sub> by using the

low-thermal gradient Czochralski technique in a platinum crucible is ongoing [22]. The produced crystals have been deployed in the underground facility DAMA/R&D at the Gran Sasso laboratory (LNGS) [11, 12, 20, 21]. Measurements and R&D studies have shown the competitiveness of  $\text{ZnWO}_4$  scintillators for a DM experiment based on directionality. In fact, the light output and the time profile of the scintillation pulse for heavy particles depends on the direction of such particles with respect to the crystal axes while no difference is observed for  $\gamma/\beta$  radiation [10]. The shape of the scintillation pulse is also different for  $\gamma(\beta)$  radiation and  $\alpha$ . This pulse shape discrimination capability can potentially be of interest not only for a DM experiment but also for double beta decay searches. The  $\text{ZnWO}_4$  offers also a high atomic weight and the possibility to realize single crystals with masses of some kg [22]. Moreover, the presence of three target nuclei with very different masses (Zn, W and O) makes these scintillators sensitive to both small and large mass DM candidates, as also the  $\text{NaI(Tl)}$  is. The recently developed  $\text{ZnWO}_4$  scintillators have very good level of radiopurity. The measured upper limits are:  $20 \mu\text{Bq/kg}$  for the  $^{40}\text{K}$ ,  $2 \mu\text{Bq/kg}$  for the  $^{226}\text{Ra}$  and in the range  $(0.17\text{-}1.3) \mu\text{Bq/kg}$  for the  $^{228}\text{Th}$  [11, 14].

A further radio-purification of  $\text{ZnWO}_4$  crystal scintillators is feasible. The R&D is still ongoing.

As confirmed by the measurements performed at LNGS, the crystals have relatively high light output at room temperature, being about 20% of the  $\text{NaI(Tl)}$  scintillator. It appears feasible to improve the light output of the crystal considering that it can increase when working at low temperature [23]. To study this feature, a small cryostat is currently under test at LNGS to implement and optimize the cooling system; this system will allow to reach a stable working temperature around  $-50^\circ\text{C}$ .

In order to employ the  $\text{ZnWO}_4$  for DM investigation with the directionality approach, it is crucial to measure and quantify the anisotropy of the scintillator for nuclear recoils. For this purpose a campaign of measurements has been recently performed by using a 7.99 g mass  $\text{ZnWO}_4$  crystal scintillator of  $(10 \times 10 \times 10.4) \text{ mm}^3$ , in the framework of the ADAMO project [19]. The crystal has been obtained by a second crystallization procedure using low-thermal gradient Czochralski technique from zinc tungstate crystals made from tungsten oxide additionally purified by double sublimation of tungsten chlorides [24]. The crystallographic axes were identified by the producer and experimentally verified.

Before measuring the response of the  $\text{ZnWO}_4$  crystal with a monochromatic neutron source at ENEA-CASACCIA, the crystal has been irradiated with  $\alpha$  particles at LNGS. In the following the obtained results are briefly reported, while more details can be found in [19].

### 3 Measurements with $\alpha$ particles

The  $\text{ZnWO}_4$  crystal  $(10 \times 10 \times 10.4 \text{ mm}^3)$  has been coupled to a Hamamatsu H11934-200 PMT (Ultra Bialkali photocathode with an effective area of  $23 \times 23 \text{ mm}^2$  and quantum efficiency  $\simeq 43\%$  at 400 nm and  $\simeq 25\%$  at 500 nm). The scintillation profiles coming from the detector have been recorded by a LeCroy WaveSurf24X-sA oscilloscope (4 chn, 2.5 GSamples/s, 200 MHz) in a time window of  $100 \mu\text{s}$ . The measurements have been performed by using an  $^{241}\text{Am}$  source and various sets of thin mylar films as absorbers to decrease the  $\alpha$  particles energy. The beam of  $\alpha$  particles has been collimated before reaching the crystal face. The energies of  $\alpha$  beam have been measured with a CANBERRA Alpha Spectrometer (model 7401VR). The energy scale of the crystal for each measurement has been calibrated by using  $^{137}\text{Cs}$  and  $^{22}\text{Na}$   $\gamma$  sources.

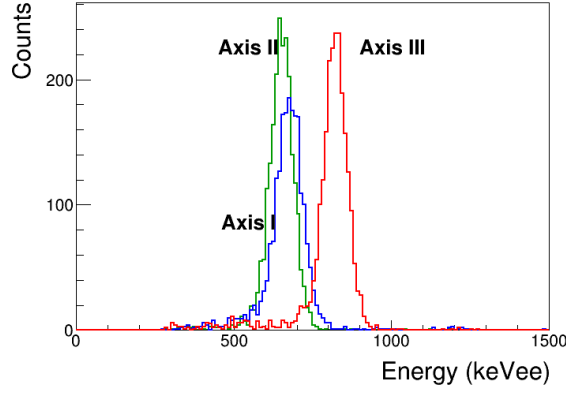


**Figure 1.** Energy spectra of 4.63 MeV  $\alpha$  particles impinging along the three axes of the crystal.

The typical energy distributions of the  $\alpha$  particles impinging along the three axes of the crystal are shown in Fig. 1. The  $\text{ZnWO}_4$  crystal was irradiated in the directions perpendicular to the (100), (001) and (010) crystal planes: hereafter crystal axes I (blue on-line), II (green on-line) and III (red on-line), respectively in Fig. 1 and in Fig. 2.

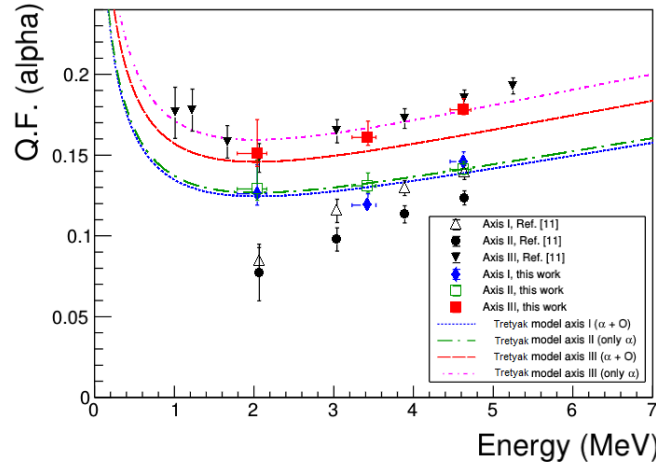


**Figure 2.** Dependence of the  $\alpha/\beta$  ratio on the energy of the  $\alpha$  particles measured with a  $\text{ZnWO}_4$  scintillator in Ref. [10] (black points) compared with those reported in this paper (colored points). The anisotropic behavior of the crystal is evident. The models for each crystal axis, obtained following the prescription of Ref. [25] are also reported. The curves have been obtained by fitting the data from  $\alpha$ 's and from recoils or only from  $\alpha$ 's.

In Figure 2 the dependence of the  $\alpha/\beta$  ratio<sup>1</sup> as a function of energy for the three different directions of the  $\alpha$  beam relatively to the crystal planes is shown. In particular, the quenching factor for  $\alpha$  particles measured along the crystal axis III is about 1.2 times larger than that measured along the crystal axes I and II. Instead, the quenching factors measured along the crystal axes I and II are quite similar. The error bars are mainly due to the uncertainty of the alpha energy which is slightly degraded in air.

<sup>1</sup> $\alpha/\beta$  ratio (for  $\alpha$  particles) and quenching factor (for ions in general) are determined as the ratio of particle's energy measured in scale calibrated with  $\beta$  or  $\gamma$  sources to the real energy of the particle.

The quenching factors and the anisotropic effect reported here are in reasonable agreement with those of Ref. [10], as shown in Fig. 2; in the figure the behavior of the  $\alpha/\beta$  ratio as expected for each crystal axis in the model of Ref. [25] is also reported. The curves have been obtained by fitting the data from  $\alpha$ 's and from recoils or only from  $\alpha$ 's.

Therefore, the data confirm the anisotropic features of  $\text{ZnWO}_4$  crystal scintillator in case of  $\alpha$  particles.

#### 4 Measurements with neutrons

Monochromatic neutrons have been generated by the Thermo Scientific portable generator MP 320. Neutrons are produced in the  $d(t, \alpha)n$  reaction with energy around 14.7 MeV by accelerating deuterons toward a tritium target in electric potential. For the requirements of the experiment a configuration with beam acceleration voltage of 60 kV and a beam current of 40  $\mu\text{A}$  have been adopted in order to maximize the neutron yield and the stability of the beam operation; the production rate was around  $10^7$  n/s. In the experimental setup, neutrons leaving the target at 90 degrees to the forward direction have been used; at this angle, simple kinematics predicts a value  $E_n = 14.05$  MeV for a beam acceleration voltage of 60 kV.

In a single elastic scattering of neutrons with target nuclei, nuclear recoils are induced, and the scattered neutron is detected by two neutron detectors placed at a given scattering angle. In such a configuration the energy and the direction of the recoiling nucleus is fixed and, by measuring the energy released in the  $\text{ZnWO}_4$  detector – in keV electron equivalent (keVee) – it is possible to determine the quenching factor. By changing the crystal axes orientation, the quenching factor for the different axes can be measured.

A scheme of the set-up is shown in Fig. 3. The  $\text{ZnWO}_4$  detector is placed in front of the neutron

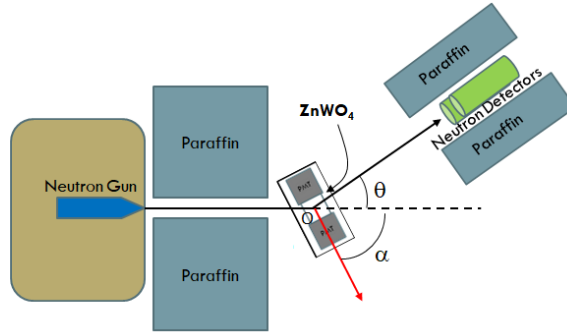


**Figure 3.** Schematic view from the top of the experimental set-up. The two neutron detectors are one above the other.

channel on a revolving platform around a vertical axis ( $O$  axis), allowing us to fix the direction of the crystal axis with respect to the impinging neutrons: the  $\alpha$  angle as depicted in Fig. 3. The  $\text{ZnWO}_4$  crystal is centered on the  $O$  axis and is optically coupled to two Hamamatsu H11934-200 PMTs on opposite faces. In the set-up, the PMTs are on the faces perpendicular to the crystal axis III; thus,  $\alpha$  identifies the angle between the crystal axis III and the impinging neutrons direction. The crystal axis I is also on the horizontal plane, while the axis II is vertical. The  $\text{ZnWO}_4$  crystal and the two PMTs are inside a black plastic box. The neutrons scattered off the  $\text{ZnWO}_4$  crystal are tagged by two neutron detectors by Scionix employing EJ-309 liquid scintillator. The EJ-309 scintillator has

a very high capability to discriminate neutrons interactions from the gamma background by Pulse Shape Discrimination (PSD). The neutron detectors are placed 82 cm far from  $O$  axis, one above the other to maintain the same neutron scattering angle  $\theta$  (see Fig. 3) and to improve the solid angle acceptance. They are held by an arm and free to rotate around the  $O$  axis.

The signals from the two PMTs coupled to the  $\text{ZnWO}_4$  detector are summed and recorded by a CAEN DT5720 transient digitizer with 250 MS/s sample rate. The trigger is obtained by the coincidence between a signal in the  $\text{ZnWO}_4$  detector and in the EJ-309 detectors within a time window of  $\pm 500$  ns.

The energy detected by the  $\text{ZnWO}_4$  detector is evaluated from the digitized pulse area.  $^{133}\text{Ba}$  and  $^{137}\text{Cs}$  sources were used to calibrate the detector energy scale. The typical energy resolution was  $\sigma/E = 4.4\%$  at the 662 keV  $\gamma$  peak. The energy calibration has been performed before and after neutron irradiation.

Neutron events in the EJ-309 detectors have been selected by a PSD data analysis based on: i) head/tail analysis; ii) analysis of the mean time,  $\tau$ , of the time profile of the pulse. A typical example of the separation between gamma and neutrons exploiting the two techniques is reported in Fig. 4-left and in Fig. 4-right, respectively.

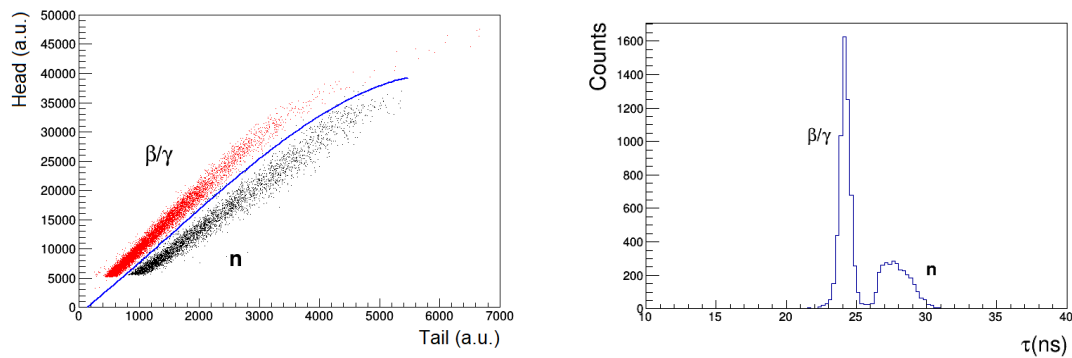


**Figure 4.** Example of gamma/neutron separation by PSD in EJ-309 liquid scintillator. Left: head/tail analysis. Right: distribution of the mean time,  $\tau$ , variable.

To select the nuclear recoils induced by the elastic scattering of neutrons over the background, an important quantity is the time passing between the signals in the  $\text{ZnWO}_4$  detector and the neutron detectors EJ-309 (Time of Flight,  $TOF$ ). A variable  $\Delta t = t_0^{EJ} - t_0^{ZWO}$ , can be defined where  $t_0^{EJ}$  ( $t_0^{ZWO}$ ) is the starting time of the EJ-309 ( $\text{ZnWO}_4$ ) pulse. The transit time of the neutron detectors PMT is  $\approx 40$  ns while it is  $\approx 6$  ns for the Hamamatsu H11934-200. The  $\Delta t$  variable is shifted with respect to  $TOF$  and it has been calibrated considering the coincidences between high energy events in the  $\text{ZnWO}_4$  detector and gamma events in the neutron detectors. An interval  $\Delta t \approx 34$  ns has been obtained from the data; it is in agreement with the expectation. This  $TOF$  calibration has been taken into account in the analysis.

For a fixed scattering angle  $\theta$  and crystal axis, the event pattern searched for was represented by a scintillation pulse in the  $\text{ZnWO}_4$  detector in coincidence with a neutron in the EJ-309 detectors.

In Fig. 5-left the  $TOF$  distribution is depicted for the case of  $\theta = 70^\circ$  and crystal axis I, while in Fig. 5-right is shown the bi-dimensional plot  $TOF$  vs  $\text{ZnWO}_4$  energy ( $E$  is in keVee). These plots show a continuum due to random coincidences, a clear excess of events with energy around

80 keVee, and  $TOF$  in agreement with the expectation for scattered neutrons on target nuclei. The peak in the  $TOF$  variable shows a tail on the left due to the first photoelectron delay in  $ZnWO_4$  (effective average scintillation decay time  $\approx 24 \mu s$ ). The observed excess can be ascribed to the O recoils in the  $ZnWO_4$  detector and its position provides the quenching factor of this nucleus for the scattering-angle and crystal-axis used. The Zn and W recoils are expected to be well below the energy threshold that has been used in the present experimental conditions.

The behavior of the  $TOF$  distribution can be explained by considering that events belong to the sum of two main contributions: 1) one due to the coincidences caused by the elastic scatterings of neutrons on the oxygen nuclei, and 2) the random flat coincidences ( $f_{rnd}$ ). To build a model for the  $TOF$  behavior, some assumptions can be considered: i) the signal of the neutron detectors is "prompt" (that is the time delay between the neutron interaction and the starting time of the EJ-309 pulse is mostly equal to the PMT transit time); ii) the  $ZnWO_4$  time delay between the neutron interaction and the starting time of the pulse is given by the PMT transit time plus the delay of the first photoelectron in the  $ZnWO_4$  detector (effective average scintillation decay time  $\approx 24 \mu s$  [10]); iii) the probability to have the first photoelectron in  $ZnWO_4$  at time  $t$  is  $\frac{1}{\tau} e^{-t/\tau}$ , where  $\tau$  is a free parameter linked to the effective scintillation decay time and the number of available photoelectrons; iv) the fluctuations of the transit times of the PMTs of the  $ZnWO_4$  and of EJ-309 detectors, and the time resolution of the digitizer (2 ns bin size for the neutron detectors and 4 ns for the  $ZnWO_4$  detector) are taken into account by making a convolution of the time distribution with a Gaussian function having a characteristic spread  $\sigma$ . Thus, the model function of  $TOF$  can be written as:

$$f(TOF|f_{rnd}, A, \tau, \sigma, TOF_0) = f_{rnd} + A \int_0^{\infty} e^{-x/\tau} e^{-\frac{(x+TOF-TOF_0)^2}{2\sigma^2}} dx \quad (4.1)$$

where  $TOF_0$  represents the expectation value of the neutrons time of flight and  $A$  is a normalization factor. By solving the integral one gets:

$$f(TOF) = f_{rnd} + B e^{-\frac{TOF_0-TOF}{\tau}} \left[ 1 - \operatorname{erf} \left( -\frac{TOF_0-TOF}{\sqrt{2}\sigma} + \frac{\sigma}{\sqrt{2}\tau} \right) \right] \quad (4.2)$$

where  $B$  includes only constant factors:  $B = A \sqrt{\frac{\pi}{2}} \sigma e^{\frac{\sigma^2}{2\tau^2}}$ . The result of the  $TOF$  distribution fits with the function given in eq. 4.2 is plotted in Fig. 5-left; it gives:  $f_{rnd} \approx 5.5$  counts/ 5 ns,  $B \approx 21.6$  counts/ 5 ns,  $\tau \approx 16.9$  ns,  $\sigma \approx 5.8$  ns and  $TOF_0 \approx 15.4$  ns. The model reproduces well the experimental data and is in good agreement with the expectations. A Monte Carlo simulation gives similar results.

For the estimation of the quenching factors three scattering angles were considered. Since the responses of the crystal axes I and II are rather similar, only the case of axis I was considered. Figure 6 shows an example of the energy distributions of the detected energy,  $E$ , in the  $ZnWO_4$  detector, measured in keVee, ( $\theta = 70^\circ$  and axes III and I). Two distributions are reported for each plot: one is obtained by selecting events in the time window expected for the  $TOF$  of neutrons elastically scattered off the nuclei of  $ZnWO_4$  detector,  $-20 \text{ ns} < TOF < 30 \text{ ns}$  (light red histogram); the other is presented by selecting off-window events (random coincidences),  $60 \text{ ns} < TOF < 110 \text{ ns}$  (blue histogram). The off-window events are related to random coincidences and, therefore, their distribution is the background distribution in the histogram of the in-window events. The peaks are

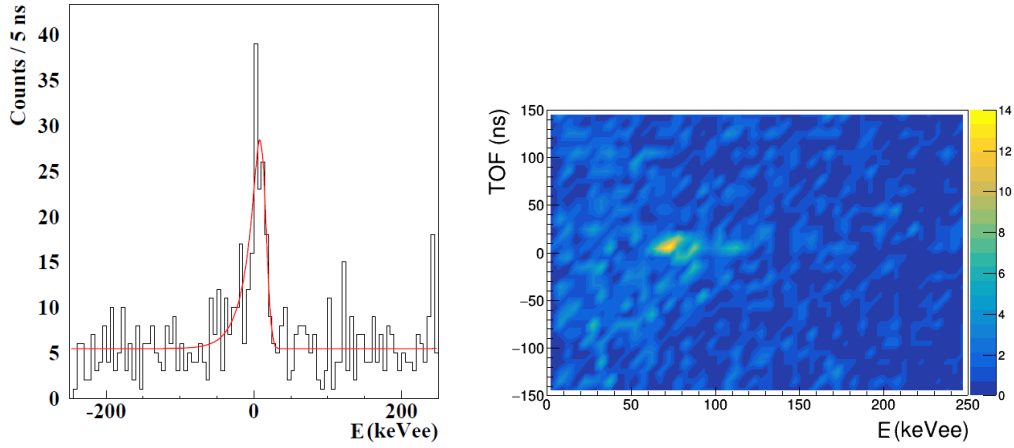


**Figure 5.** *TOF* distribution and bi-dimensional plot *TOF* vs  $\text{ZnWO}_4$  energy (in keVee) for coincidences obtained after selecting neutrons in the neutron detectors, for the case of scattering angle  $\theta = 70^\circ$  and axis I. Left: The *TOF* distribution shows a continuum due to random coincidences and a clear peak, that is in agreement with the expected *TOF* for neutrons after elastic scattering off the nuclei of  $\text{ZnWO}_4$  detector. The peak shows a tail on the left part due to the first photoelectron delay in  $\text{ZnWO}_4$ . The fit with the function of eq. 4.2 is superimposed (see text). Right: A clear peak is present at the proper value of *TOF* and at the given energy. The peak position in the distribution measured by the  $\text{ZnWO}_4$  detector provides the quenching factor of the O nucleus for the scattering-angle and crystal-axis used.

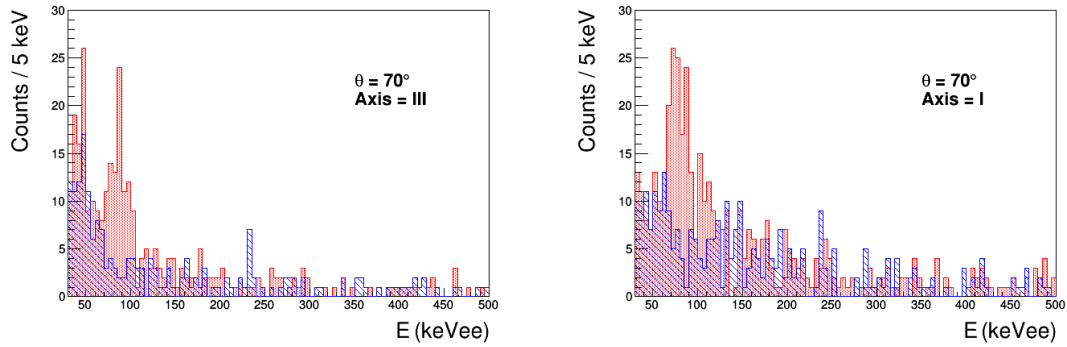


**Figure 6.** Energy spectra measured by the  $\text{ZnWO}_4$  detector (in  $\gamma$  scale, keVee) for the case of  $\theta = 70^\circ$  and axes III and I. Only events identified as neutrons in the neutron detectors are selected. Light (red on-line) histogram: events selected in the proper window of the *TOF* variable ( $-20 \text{ ns} < \text{TOF} < 30 \text{ ns}$ ). Dashed (blue on-line) histogram: events selected in the off-window ( $60 \text{ ns} < \text{TOF} < 110 \text{ ns}$ ).

evident and can be ascribed to the oxygen nuclear recoils. The positions of the peaks are obtained by fitting them with a Gaussian curve plus an exponential function, that simulates the background of the random coincidences. The energy resolutions,  $\sigma$ , of the peaks are between 8 and 12 keVee; the values are well in agreement with the energy dependence:  $\sigma \propto \sqrt{E}$ .

In Table 1 the summary of the peak positions measured for the three considered angles is reported. The expected recoil energies for the oxygen nucleus,  $E_{R,O}$ , are also given. The obtained quenching factors are calculated as the ratio  $E/E_{R,O}$  and the last column reports the degree of anisotropy for each scattering-angle/recoil energy.

In Fig. 7 the obtained value for the quenching factors are plotted together with the models for the considered crystal axes derived from Ref. [25]. This parameter has been estimated, for each

**Table 1.** Summary table of the peak position due to oxygen nuclear recoils. For each scattering angle,  $\theta$ , and for the different axes of the  $\text{ZnWO}_4$  crystal, the peak position,  $E$ , the energy resolution,  $\sigma$ , the expected recoil energies for the oxygen nucleus,  $E_{R,O}$ , the quenching factors,  $Q$ , and the anisotropy,  $Q_{III}/Q_I$  ratio, are reported.

Scattering angle, $\theta$	Crystal axis	$E$ (keVee)	$\sigma$ (keVee)	$E_{R,O}$ (keV)	Quenching factor, $Q$	$Q_{III}/Q_I$
80°	III	$99.3 \pm 2.5$	9	1402	$0.0708 \pm 0.0018$	$1.174 \pm 0.051$
	I	$84.5 \pm 2.9$	12		$0.0603 \pm 0.0021$	
70°	III	$86.5 \pm 2.0$	7	1128	$0.0767 \pm 0.0018$	$1.121 \pm 0.038$
	I	$77.2 \pm 1.9$	10		$0.0684 \pm 0.0017$	
60°	III	$75.4 \pm 1.8$	9	866	$0.0871 \pm 0.0021$	$1.166 \pm 0.059$
	I	$64.7 \pm 2.9$	10		$0.0747 \pm 0.0033$	

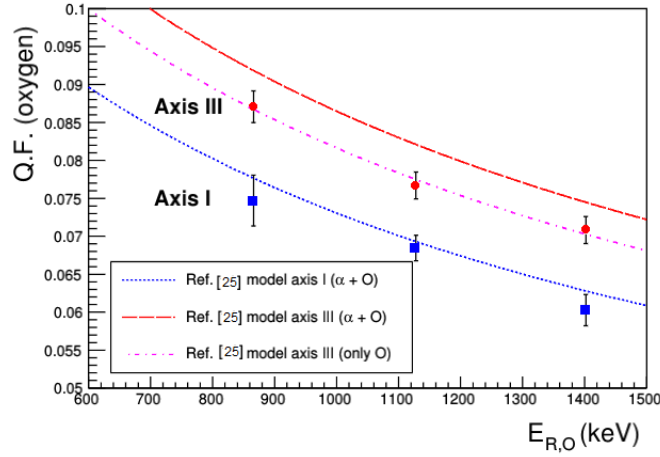


**Figure 7.** Quenching factors for oxygen nuclear recoils in  $\text{ZnWO}_4$  for the crystal axes I and III as function of the expected recoil energies  $E_{R,O}$ . In the plot the expected behavior of quenching factor for the two crystal axes of the model of Ref. [25] are also reported; they have been obtained by fitting the data of the  $\alpha$ 's and oxygen recoil data together, and oxygen recoil data only.

axis, taking into account the response of  $\text{ZnWO}_4$  to  $\alpha$  particles and to oxygen recoils (see Ref. [19]).

## 5 Conclusions

The development and the results obtained with a  $\text{ZnWO}_4$  scintillation detector and reported here demonstrate that this anisotropic scintillator is very promising to exploit the directionality technique to investigate those DM particle inducing recoils of target nuclei.

The results confirm the anisotropic response of the  $\text{ZnWO}_4$  crystal scintillator to  $\alpha$  particles and to oxygen nuclear recoils. The presence of a good anisotropic response also in the lower energy region is supported by the trend of the measured quenching factors. This could open the possibility to realize a pioneer ADAMO experiment to investigate the mentioned DM candidates by means of directionality through the use of anisotropic scintillators.

## References

- [1] R. Bernabei et al., *La Rivista del Nuovo Cimento* **26 n.1** (2003) 1.
- [2] R. Bernabei et al., *Eur. Phys. J. C* **56** (2008) 333.
- [3] R. Bernabei et al., *Eur. Phys. J. C* **67** (2010) 39.
- [4] R. Bernabei et al., *Eur. Phys. J. C* **73** (2013) 2648.
- [5] R. Bernabei et al., *Nucl. Phys. At. Energy* **19** (2018) 307.
- [6] R. Bernabei et al., *Nucl. Phys. At. Energy* **20** (2019) 317.
- [7] P. Belli et al., *Nuovo Cimento C* **15** (1992) 475.
- [8] R. Bernabei et al., *Eur. Phys. J. C* **28** (2003) 203.
- [9] F. Cappella et al., *Eur. Phys. J. C* **73** (2013) 2276.
- [10] F.A. Danevich et al., *Nucl. Instrum. Methods A* **544** (2005) 553.
- [11] P. Belli et al., *Nucl. Instrum. Methods A* **626-627** (2011) 31.
- [12] P. Belli et al., *J. Phys. G* **38** (2011) 115107.
- [13] A.S. Barabash et al., *Nucl. Instrum. Methods A* **833** (2016) 77.
- [14] P. Belli et al., *Nucl. Instrum. Methods A* **935** (2019) 89.
- [15] R. Cerulli, *Int. J. of Mod. Phys. A* **32** (2017) 1743009.
- [16] R. Bernabei et al., *AIP Conference Proceedings* **1549** (2013) 189.
- [17] V. Caracciolo et al., *J. Phys. Conf. Ser.* **718** (2016) 042011.
- [18] R. Bernabei et al., *EPJ Web of Conferences* **136** (2017) 05002.
- [19] R. Bernabei et al., *Eur. Phys. J. A* **56** (2020) 83.
- [20] P. Belli *et al.*, *Phys. Lett. B* **658** (2008) 193.
- [21] P. Belli *et al.*, *Nucl. Phys. A* **826** (2009) 256.
- [22] E.N. Galashov *et al.* *Functional Materials* **16** (2009) 63.
- [23] L.L. Nagornaya *et al.*, *IEEE Trans. Nucl. Sci.* **56** (2009) 2513.
- [24] V.N. Shlegel et al., *JINST* **12** (2017) C08011.
- [25] V.I. Tretyak, *Astropart. Phys.* **33** (2010) 40.